

Design, synthesis, and biological evaluation of novel chrysin derivatives as poly(ADP-ribose) polymerase 1 (PARP1) inhibitors for the treatment of breast cancer

Yao YANG, Jing TONG, Xianshun XIE, Hong CAO, Yong FU, Yong LUO, Shan LIU, Wen CHEN, Ning YANG

Citation: Yao YANG, Jing TONG, Xianshun XIE, Hong CAO, Yong FU, Yong LUO, Shan LIU, Wen CHEN, Ning YANG, Design, synthesis, and biological evaluation of novel chrysin derivatives as poly(ADP-ribose) polymerase 1 (PARP1) inhibitors for the treatment of breast cancer, *Chinese Journal of Natural Medicines*, 2024, 22(5), 455–465. doi: [10.1016/S1875-5364\(24\)60642-4](https://doi.org/10.1016/S1875-5364(24)60642-4).

View online: [https://doi.org/10.1016/S1875-5364\(24\)60642-4](https://doi.org/10.1016/S1875-5364(24)60642-4)

Related articles that may interest you

Promising natural lysine specific demethylase 1 inhibitors for cancer treatment: advances and outlooks

Chinese Journal of Natural Medicines. 2022, 20(4), 241–257 [https://doi.org/10.1016/S1875-5364\(22\)60141-9](https://doi.org/10.1016/S1875-5364(22)60141-9)

Recent progress on betulinic acid and its derivatives as antitumor agents: a mini review

Chinese Journal of Natural Medicines. 2021, 19(9), 641–647 [https://doi.org/10.1016/S1875-5364\(21\)60097-3](https://doi.org/10.1016/S1875-5364(21)60097-3)

Natural products as potent inhibitors of hypoxia-inducible factor-1 α in cancer therapy

Chinese Journal of Natural Medicines. 2020, 18(9), 696–703 [https://doi.org/10.1016/S1875-5364\(20\)60008-5](https://doi.org/10.1016/S1875-5364(20)60008-5)

Design and semisynthesis of oleanolic acid derivatives as VEGF inhibitors: Inhibition of VEGF-induced proliferation, angiogenesis, and VEGFR2 activation in HUVECs

Chinese Journal of Natural Medicines. 2022, 20(3), 229–240 [https://doi.org/10.1016/S1875-5364\(22\)60159-6](https://doi.org/10.1016/S1875-5364(22)60159-6)

Novel carbohydrate-triazole derivatives as potential α -glucosidase inhibitors

Chinese Journal of Natural Medicines. 2020, 18(10), 729–737 [https://doi.org/10.1016/S1875-5364\(20\)60013-9](https://doi.org/10.1016/S1875-5364(20)60013-9)

cDNA cloning of a novel lectin that induce cell apoptosis from *Artocarpus hypargyreus*

Chinese Journal of Natural Medicines. 2021, 19(2), 81–89 [https://doi.org/10.1016/S1875-5364\(21\)60009-2](https://doi.org/10.1016/S1875-5364(21)60009-2)



Wechat

•Original article•

Design, synthesis, and biological evaluation of novel chrysin derivatives as poly(ADP-ribose) polymerase 1 (PARP1) inhibitors for the treatment of breast cancer

YANG Yao^{1,2Δ}, TONG Jing^{2Δ}, XIE Xianshun⁴, CAO Hong⁵, FU Yong³, LUO Yong², LIU Shan²,
CHEN Wen³, YANG Ning^{1,3*}¹ Hengyang Medical School, University of South China, Hengyang 421200, China;² Emergency Department, Hengyang Medical School, The Second Affiliated Hospital, University of South China, Hengyang 421200, China;³ Hengyang Medical School, The Second Affiliated Hospital, University of South China, Hengyang 421200, China;⁴ Hemato-oncology Department, Hengyang Medical School, The Second Affiliated Hospital, University of South China, Hengyang 421200, China;⁵ Department of Breast and Thyroid Surgery, Hengyang Medical School, The Second Affiliated Hospital, University of South China, Hengyang 421200, China

Available online 20 May, 2024

[ABSTRACT] In this study, we reported the discovery and structure-activity relationship analysis of chrysin derivatives as a new class of inhibitors targeting poly (ADP-ribose) polymerase 1 (PARP1). Among these derivatives, compound **5d** emerged as the most effective chrysin-based inhibitor of PARP1, with an IC₅₀ value of 108 nmol·L⁻¹. This compound significantly inhibited the proliferation and migration of breast cancer cell lines HCC-1937 and MDA-MB-436 by inducing DNA damage. Furthermore, **5d** induced apoptosis and caused an extended G₁/S-phase in these cell lines. Molecular docking studies revealed that **5d** possesses a strong binding affinity toward PARP1. *In vivo*, in a xenograft model, **5d** effectively reduced tumor growth by downregulating PARP1 expression. Overall, compound **5d** shows promise as a potential therapeutic agent for the treatment of BRCA wild-type breast cancer.

[KEY WORDS] Chrysin derivatives; PARP1; Antitumor; DNA damage; Small molecules

[CLC Number] R284, R965 **[Document code]** A **[Article ID]** 2095-6975(2024)05-0455-11

Introduction

Natural products are a significant source of leads in drug discovery, as evidenced by numerous studies [1, 2]. Chrysin, a natural flavonoid, is known for its wide range of biological activities, including antibacterial, anti-inflammatory, antioxidant, anti-allergic, and antitumor effects [3, 4]. There is a growing body of evidence indicating that chrysin exerts a broad spectrum of antitumor effects by targeting multiple molecules and their associated pathways [5, 6]. For instance, CHEN *et al.* demonstrated that chrysin could inhibit the fo-

cal adhesion kinase (FAK)-regulated signaling pathways, thereby suppressing the malignant progression of tumor cells [7]. Additionally, in tumor cells, chrysin has been shown to impede proliferation, migration, and invasion by up-regulating the expression of ten-eleven translocation 1 and 5-hydroxymethylcytosine [8]. However, the therapeutic potential of chrysin is hindered by its poor aqueous solubility and low bioavailability. To overcome these limitations, researchers have developed several chrysin derivatives aimed at enhancing its antitumor efficacy under physiological conditions. In 2020, CHEN *et al.* synthesized a series of aromatic or long-chain chrysin derivatives [9]. Following this, in 2021, LI *et al.* introduced a series of chrysin derivatives incorporating amino acids [10, 11]. These derivatives have shown improved *in vitro* efficacy against various tumor cell types compared to chrysin, underscoring the value of chrysin derivatization as a strategy for developing more effective antitumor treatments.

Benzimidazole and its derivatives are recognized for their significant biological activity, particularly as nitrogen-

[Received on] 12-Dec.-2023

[Research funding] This work was supported by the Clinical Research Center for Breast & Thyroid Disease Prevention in Hunan Province (No. 2018SK4001) and the Scientific Research Project of Hunan Provincial Health Commission (No. 20201969).

[*Corresponding author] E-mail: yangning@usc.edu.cn

^ΔThese authors contributed equally to this work.

These authors have no conflict of interest to declare.

containing heterocycles. These compounds have found application in treating various tumor types [12, 13]. Notably, veliparib, which features the 1*H*-benzimidazole-4-carboxamide scaffold, is a potent and orally bioavailable inhibitor of poly (ADP-ribose) polymerase 1 (PARP1) [14]. There has been increasing interest in veliparib due to its effectiveness in treating breast and ovarian cancers deficient in the breast cancer susceptibility gene 1 (*BRCA1*) [15, 16]. Veliparib has demonstrated promising clinical outcomes in breast cancer, especially in ongoing studies of its use as monotherapy in metastatic breast cancer. Structural biology studies have highlighted the central role of the 1*H*-benzimidazole-4-carboxamide moiety as the main pharmacophore in veliparib's activity. Therefore, incorporating this functional group into chrysin may enhance its antitumor efficacy and improve its physicochemical properties, leveraging the recognized importance of the 1*H*-benzimidazole-4-carboxamide structure.

In this research, a novel series of chrysin derivatives was synthesized by introducing the 1*H*-benzimidazole-4-carboxamide group. These compounds were then screened *in vitro* for their inhibitory effects on breast cancer cell growth and PARP1 enzyme activity. Among these, molecule **5d** emerged as a notable PARP1 inhibitor. In tumor cells, **5d** demonstrated significant antiproliferative and antimigration effects by inducing DNA damage. Docking simulation studies further confirmed that **5d** fits well within the active site of the PARP1 enzyme. *In vivo* studies using a xenograft model showed that **5d** effectively inhibited tumor growth by down-regulating PARP1 expression. These results collectively suggest that **5d** is a potential lead compound for targeting PARP1.

Results and Discussion

Design and synthesis

Veliparib, recognized as a potent and orally bioavailable inhibitor of PARP, has been reported to show effectiveness in the treatment of metastatic breast cancer [17]. The X-ray co-

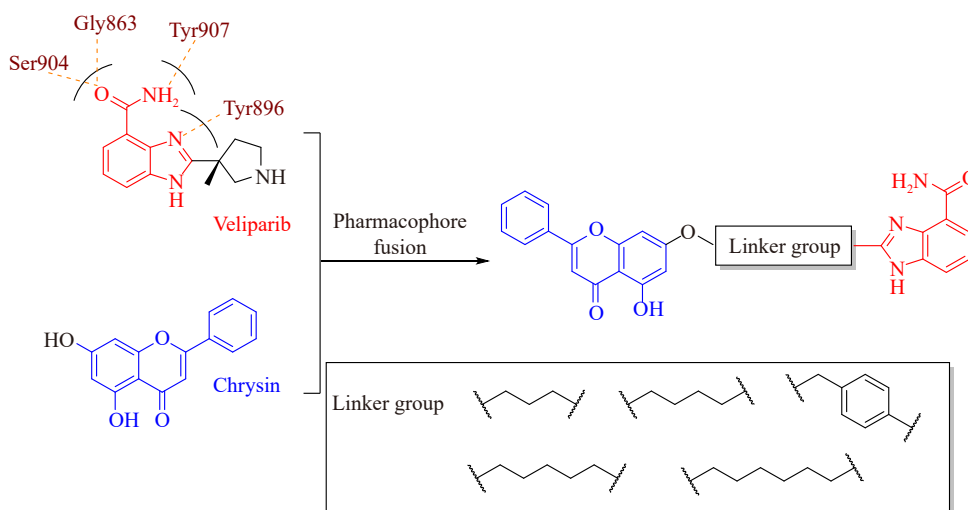
crystal structure of the veliparib-PARP complex (PDB: 7KK6) revealed that the 1*H*-benzimidazole-4-carboxamide fragment of veliparib engages the nicotinamide pockets of PARP1, forming hydrogen bonds with the residues Gly863 and Ser904. Additionally, a π - π interaction between this moiety and Tyr907 was observed (Scheme 1) [18]. The critical role of the 1*H*-benzimidazole-4-carboxamide moiety in veliparib's biological efficacy suggests that modifications to this part of the molecule may not be well tolerated. Furthermore, the tetrahydropyrrole fragment of veliparib is oriented towards the solvent-accessible region, indicating a potential site for innovative drug design [19]. Based on these insights, novel chrysin derivatives were synthesized as PARP1 inhibitors using a pharmacophore fusion strategy. Specifically, compounds **5a–5e** were developed by integrating the pharmacophoric elements of veliparib into the 7-position of the chrysin scaffold.

Compounds **5b–5e** were prepared using the general procedure outlined in Scheme 2. Initially, chrysin (compound **1**) underwent a substitution reaction in the presence of potassium carbonate (K₂CO₃), potassium iodide, and ethyl bromobutyrate derivatives (**2b–2e**) or ethyl 4-(bromomethyl)benzoate (**2a**) to attach the intermediate. Afterward, compounds **3b–3e** were obtained through the alkaline hydrolysis of their corresponding precursors. Compounds **4b–4e** were then synthesized *via* an amide condensation reaction between **3b–3e** and the relevant aromatic amine. Finally, compounds **5b–5e** were obtained through intramolecular cyclization reactions. The method for synthesizing compound **5a** was identical to the procedure described above.

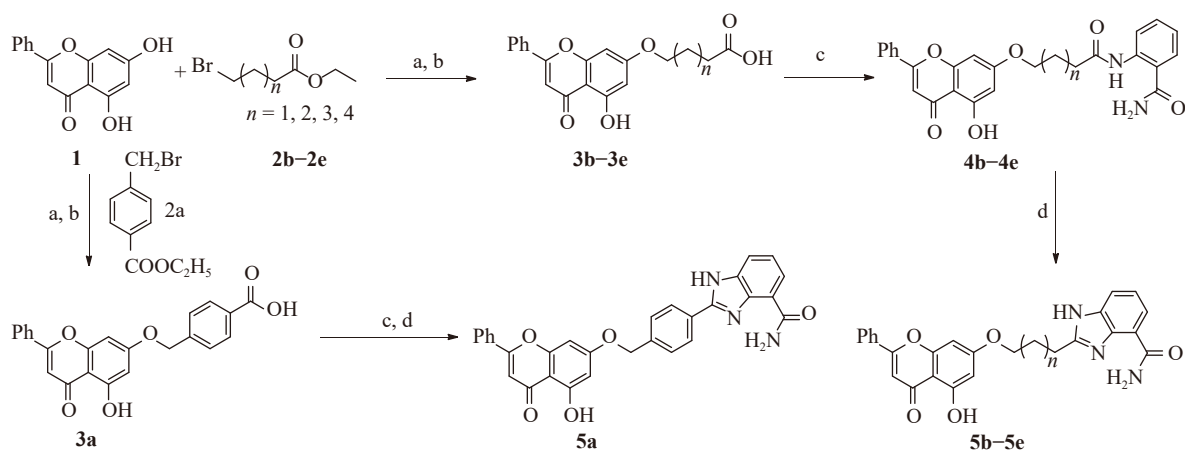
Biological activity

Structure-activity relationship of synthesized compounds

As detailed in Table 1, the study evaluated the efficacy of synthesized compounds (**5a–5e**) in inhibiting PARP1 enzymatic activity and in the antiproliferative action against breast cancer cells (including MDA-MB-231, MDA-MB-436, HCC-1937, and MCF-7). Chrysin and veliparib served as ref-

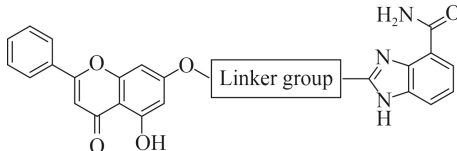


Scheme 1 Design and synthesis of novel chrysin derivatives as PARP1 inhibitors.



Scheme 2 Synthesis routes of chrysin-based PARP1 inhibitors 5a–5e. Regents and conditions: (a) K_2CO_3 , KI, acetone, 60 °C; (b) CH_3OH , NaOH, 65 °C; (c) HATU, DIPEA, DMF, 2,3-diaminobenzamide, r.t.; (d) CH_3COOH , 120 °C, reflux.

Table 1 *In vitro* inhibitory potency of compounds 5a–5e against PARP1 and breast cancer cells.

						
Compd	Linker group	PARP1 inhibitory activity ($1 \mu mol \cdot L^{-1}$, %) ^a	Antiproliferative activity (IC_{50} , $\mu mol \cdot L^{-1}$) ^b			
			MDA-MB-231	MDA-MB-436	HCC-1937	MCF-7
5a		66.9 ± 2.1	30.5 ± 0.3	28.0 ± 2.7	20.9 ± 3.3	29.8 ± 0.1
5b		74.2 ± 1.4	23.0 ± 0.6	15.6 ± 1.4	12.0 ± 0.7	25.0 ± 1.2
5c		80.2 ± 1.6	10.2 ± 0.3	14.2 ± 1.4	9.9 ± 1.7	18.2 ± 0.7
5d		93.4 ± 0.9	6.2 ± 0.6	4.5 ± 1.4	3.9 ± 0.8	14.2 ± 1.1
5e		82.7 ± 4.6	7.5 ± 1.4	7.9 ± 0.3	8.5 ± 2.0	8.6 ± 1.9
Chrysin	–	10.4 ± 3.8	> 50	> 50	> 50	> 50
Veliparib	–	96.7 ± 2.5	35.1 ± 3.8	24.4 ± 2.1	16.7 ± 1.1	37.9 ± 4.5

^aAll data were obtained by triple testing (\pm standard deviation) ^b IC_{50} values were determined from cell viability assay for 48 h.

erence compounds. The bioactivity of the target compounds appeared to be influenced by the length of the carbon chain in the linker region. Relative to chrysin, the synthesized compounds, featuring varied carbon chain lengths, exhibited enhanced efficacy against both PARP1 enzymatic activity and the proliferation of breast cancer cells. Notably, compounds **5b–5e**, with medium-length carbon chains (> 3 carbon atoms), showed significant potency against PARP1 (inhibition rates of PARP1 at $1 \mu mol \cdot L^{-1}$ exceeded 70.0%). These compounds also inhibited the growth of breast cancer cells at micromolar concentrations. Specifically, the efficacy of alkyl chain-substituted compounds (**5b–5e**) surpassed that of the benzyl-substituted compound (**5a**). This enhanced activity might be attributed to the alkyl chain facilitating interactions with amino acid residues in the binding pockets. Among these, compound **5d** was particularly noteworthy for its ex-

ceptional inhibitory effect on PARP1 (93.4% inhibition rate at $1 \mu mol \cdot L^{-1}$) and on various breast cancer cell lines (MDA-MB-231, IC_{50} 6.2 $\mu mol \cdot L^{-1}$; MDA-MB-436, IC_{50} 4.5 $\mu mol \cdot L^{-1}$; HCC-1937, IC_{50} 3.9 $\mu mol \cdot L^{-1}$; MCF-7, IC_{50} 14.2 $\mu mol \cdot L^{-1}$). Intriguingly, **5d** exhibited variable inhibitory activities across different human breast cancer cells. BRCA-deficient breast cancer cells (HCC1937 and MDA-MB-436) were more sensitive to PARP1 inhibitors than BRCA wild-type cells (MDA-MB-231 and MCF-7). Additional *in vitro* enzymatic assays revealed that **5d** demonstrated substantial potency against PARP1 with an IC_{50} value of 108 $\mu mol \cdot L^{-1}$. While **5d**'s kinase inhibitory activity was not as strong as that of veliparib, it represented a novel chrysin derivative targeting PARP1.

Binding mode of 5d into PARP1

To elucidate the selectivity of compound **5d** for PARP1,

a molecular docking study was conducted to explore its potential binding mode to PARP1. As illustrated in Fig. 1, the 1*H*-benzimidazole-4-carboxamide moiety of **5d** occupied the nicotinamide pocket of PARP1, conferring significant selectivity to the molecule. Crucially, the interactions of compound **5d** with Asp756 and Glu763 *via* hydrogen bonds were instrumental in its PARP1 inhibitory activity. The chrysin-derived functional groups of **5d** extended toward the solvent-exposed region, where the carbonyl oxygen atoms formed essential hydrogen bonds with the residues Ser904 and Gly863. Moreover, the hydrophobic bond interactions between the A and C rings of chrysin and Tyr907 further contributed to the binding affinity. Given the kinase assay data and molecular docking outcomes, compound **5d** demonstrated notable inhibitory potency against PARP1, underscoring its potential as a selective inhibitor.

Molecule 5d exerted antiproliferative and anti-migration efficacy by inhibiting the expression of PARP1 in breast cancer cells.

To investigate the impact of PARP1 activity suppression on the viability of BRCA-deficient breast cancer cells, we conducted several molecular biology experiments to assess the inhibitory effect of compound **5d** on MDA-MB-436 and HCC-1937 cell lines. Initially, the effect of **5d** on cell growth was evaluated using a colony formation assay. The results, as depicted in Fig. 2, demonstrated that compound **5d** significantly reduced the colony formation of MDA-MB-436 and HCC-1937 cells in a dose-dependent manner. Notably, at a concentration of 5 $\mu\text{mol}\cdot\text{L}^{-1}$, **5d** completely inhibited the colony formation in both MDA-MB-436 and HCC-1937 cell lines, highlighting its potent inhibitory capacity.

To further elucidate whether compound **5d** induces cell cycle arrest and promotes apoptosis in MDA-MB-436 and HCC-1937 cells, flow cytometry analysis was conducted. The results, illustrated in Fig. 3A, indicate that **5d** induced cell cycle arrest at the G₁/S phase in both HCC-1937 and MDA-

MB-436 cells. Furthermore, the percentage of apoptotic cells in HCC-1937 and MDA-MB-436 treated with **5d** at a concentration of 5 $\mu\text{mol}\cdot\text{L}^{-1}$ was 9.3% and 18.0%, respectively, as shown in (Fig. 3B). These findings suggest that **5d** effectively inhibits the proliferation of HCC-1937 and MDA-MB-436 cells by triggering apoptosis and arresting the cell cycle at the G₁/S phase. Subsequently, the anti-migration effect of **5d** was assessed using a wound healing assay. Specifically, at a concentration of 5 $\mu\text{mol}\cdot\text{L}^{-1}$, **5d** demonstrated significant potency in inhibiting the migration of MDA-MB-436 and HCC-1937 cells, as evidenced by the results presented in Fig. 4.

In our final series of experiments, we assessed the impact of compound **5d** on the expression of PARP in MDA-MB-436 and HCC-1937 cells. The results, depicted in Fig. 5B, revealed that continuous exposure to veliparib led to an accumulation of PARP1 in the nuclei of HCC-1937 and MDA-MB-436 cells, thereby increasing the expression levels of PARP1. Interestingly, a combined treatment involving

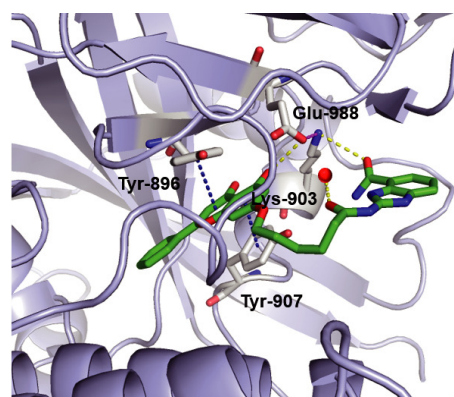


Fig. 1 Predicted binding modes of **5d** with PARP1 (PDB ID:7KK6). Hydrogen binding interactions are illustrated by yellow dashed lines. Blue dashed lines demonstrate the hydrophobic interaction.

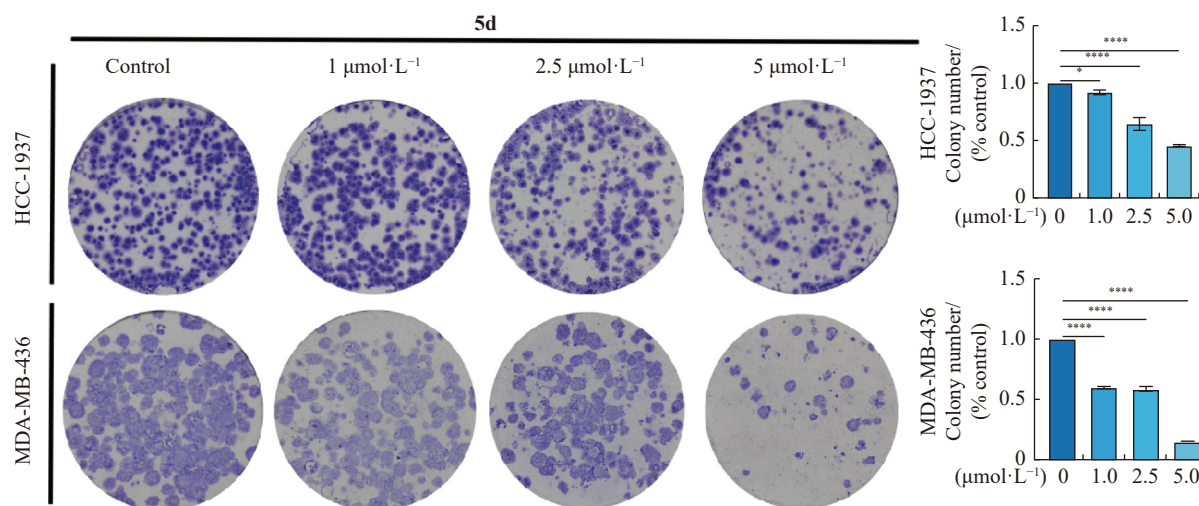


Fig. 2 Colony formation assay of MDA-MB-436 and HCC-1937 cells treated with **5d**. The error bar indicated the SD, * $P < 0.05$ and **** $P < 0.0001$ vs the control groups.

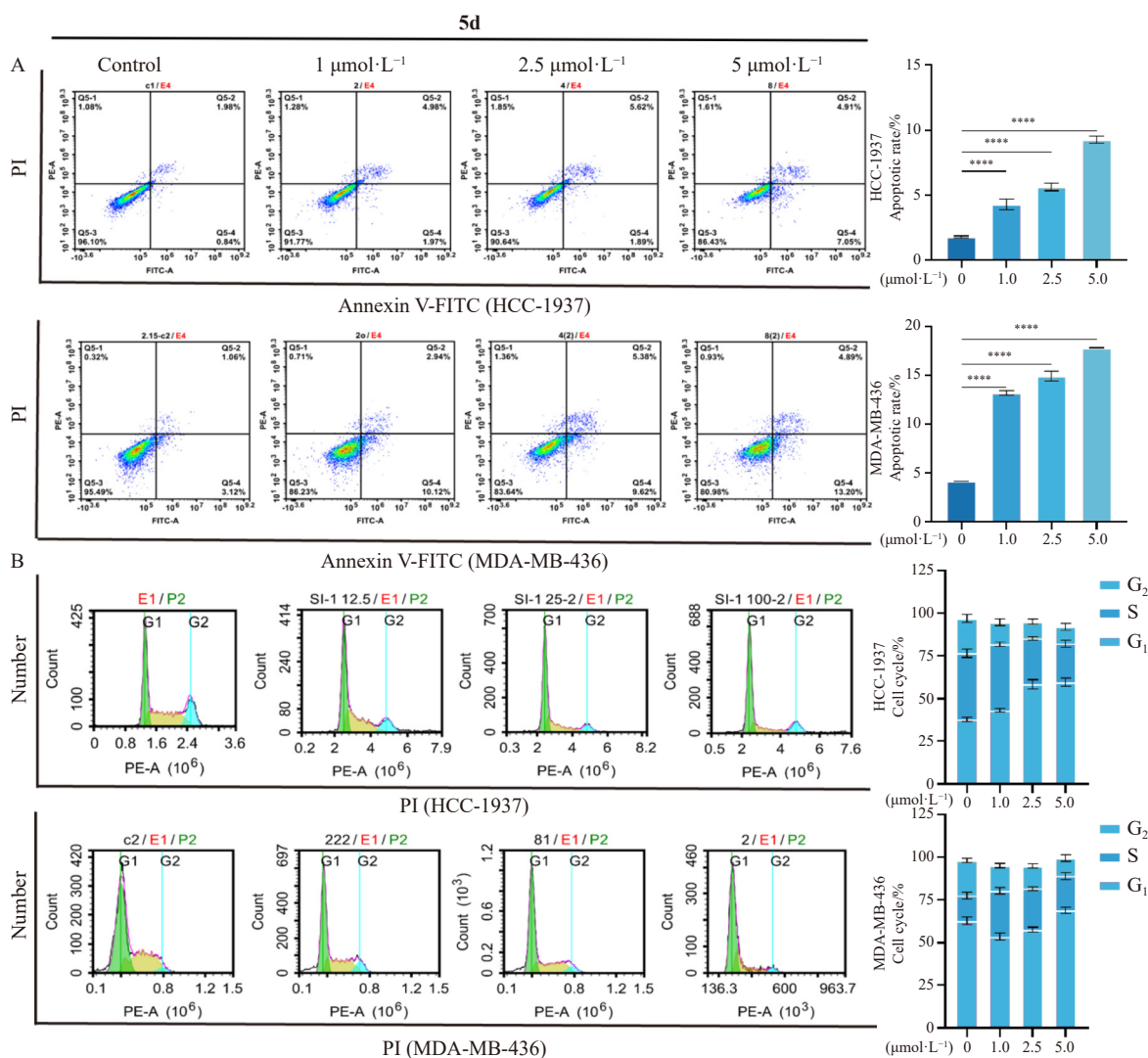


Fig. 3 Flow cytometry analysis of apoptosis and cell cycle in HCC-1937 and MDA-MB-231 cell lines. The cells were treated with **5d** at different concentrations. (A) Analysis of the cell apoptosis; (B) Cell cycle distribution diagram; the error bar indicated the SD, **** $P < 0.0001$ vs the control groups.

chrysin and veliparib also significantly reduced the expression of PARP1, although the underlying mechanism remains to be elucidated and warrants further investigation. It is hypothesized that chrysin, being a bioactive natural product with multiple targets, may engage in a synthetic lethal interaction with the PARP inhibitor veliparib, culminating in synergistic effects. Additionally, treatment with 5 $\mu\text{mol}\cdot\text{L}^{-1}$ of compound **5d** notably decreased the expression of PARP in both HCC-1937 and MDA-MB-436 cells, highlighting its potential efficacy.

Molecule 5d suppressed genes involved in DNA damage repair

The alkaline comet assay was utilized to assess DNA damage levels, evaluating the extent of damage based on tail length^[20]. Results depicted in Fig. 6 showed a significant increase in the number of comets and tail length in cells exposed to compound **5d**, indicating elevated DNA damage in a

dose-dependent manner. Further analysis focused on the inhibitory effects of **5d** on the expression of key enzymes involved in the homologous recombination (HR) repair of DNA damage, specifically BRCA and RAD51, in MDA-MB-436 and HCC-1937 cells. As illustrated in Fig. 5, exposure to 5 $\mu\text{mol}\cdot\text{L}^{-1}$ **5d** significantly reduced the expression of HR repair pathway components BRCA and RAD51 in these cell lines. These findings suggest that treatment with **5d** not only induces DNA damage but also downregulates critical factors in the DNA HR repair pathway, leading to apoptotic cell death. Additionally, γH2AX , recognized as an early marker of the DNA damage response, serves as a direct indicator of the extent of DNA damage^[21]. Immunofluorescence analysis, as shown in Fig. 7, indicated that **5d** treatment positively influenced the expression of γH2AX in MDA-MB-436 and HCC-1937 cells, with a noticeable increase observed at a concentration of 5 $\mu\text{mol}\cdot\text{L}^{-1}$. These collective results under-

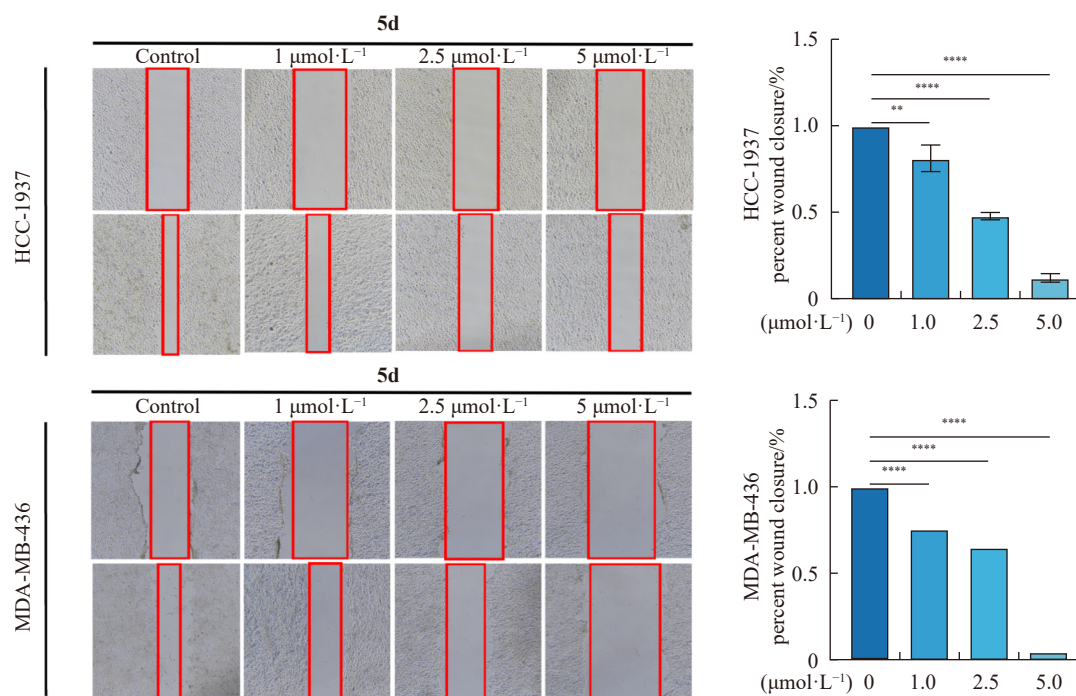


Fig. 4 *In vitro* antimigration activities of **5d**. A wound healing model was used to investigate the migration capabilities of cells. The error bar indicated the SD, ** $P < 0.01$ and **** $P < 0.0001$ vs the control groups.

score the potential of **5d** in stimulating DNA damage and inhibiting DNA repair pathways, offering a mechanistic insight and a foundational basis for the further exploration and application of chrysin derivatives.

In vivo antitumor potency

The *in vivo* antitumor efficacy of compound **5d** was assessed using an MDA-MB-436 xenograft model in nude mice. The mice, xenografted with breast cancer cells, received oral administration of **5d** at doses of 40 and 20 $\mu\text{mol}\cdot\text{L}^{-1}$, as well as chrysin at 20 $\text{mg}\cdot\text{kg}^{-1}$. Results depicted in Figs. 8A–8B demonstrated that both **5d** and chrysin significantly reduced tumor volume at the same concentration of 20 $\text{mg}\cdot\text{kg}^{-1}$. Notably, a dose of 40 $\text{mg}\cdot\text{kg}^{-1}$ **5d** exhibited the highest potency, achieving a tumor growth inhibition rate of 60.7%. Additionally, there was no significant change in the body weight of nude mice treated with **5d** compared to the control group (Fig. 8C). To further explore the mechanism of action of **5d** *in vivo*, the immunoreactivity of proliferation markers Ki-67 and PARP1 in tumor tissues was investigated. As indicated in Fig. 8D, the expression levels of both Ki-67 and PARP1 exhibited a decreasing trend in the groups treated with **5d**. These findings suggest that compound **5d** possesses promising antitumor efficacy and safety profile *in vivo*.

Experimental

Chemistry

The reagents and solvents utilized in this study were sourced commercially and used without further purification. For the purification process, silica gel (100–200 mesh) served as the medium for column chromatography. The progress of reactions was monitored using a fluorescent indicator, and

UV light (254 and 365 nm) facilitated the visualization of spots on silica gel plates. Nuclear magnetic resonance (NMR) spectra were acquired using a Bruker AV-600 spectrometer (¹H, 400 MHz; ¹³C, 101 MHz), with tetramethylsilane (TMS) acting as the internal standard. In the NMR spectra, spin multiplicities were denoted using abbreviations: singlet (s), doublet (d), triplet (t), quartet (q), multiplet (m), and doublet of doublets (dd). Coupling constants (*J*) were expressed in hertz (Hz), and chemical shifts were reported in parts per million (ppm, δ) relative to TMS. The purity of the synthesized compounds, which was determined to be higher than 95%, was verified using an analytical high-performance liquid chromatography (HPLC) instrument (Shimadzu Vietnam, Co., Ltd., Kyoto, Japan). This analysis was performed on a GL-C₁₈ reverse-phase column (4.6 mm \times 150 mm, 5 μm) employing pure water and chromatographic grade methanol as the mobile phase, conducted prior to the evaluation of biological activities. High-resolution mass spectrometry (HRMS) analyses were conducted using Agilent LC/MSD TOF mass spectrometers. Melting points were determined using a digital melting point apparatus (Thermo Scientific, CA).

2-(4-(((5-hydroxy-4-oxo-2-phenyl-4H-chromen-7-yl)oxy)methyl)phenyl)-1H-benzod[imidazole-4-carboxamide (5a)

Step 1 involved the synthesis of an intermediate compound from chrysin. Chrysin (**1**, 2 mmol) was added to a mixture containing ethyl 4-(bromomethyl)benzoate (**2a**, 2.2 mmol), potassium carbonate (4 mmol), and potassium iodide (0.2 mmol) in acetone (80 mL). The mixture was stirred and refluxed at 60 °C for 12 h. Upon completion, it was cooled to room temperature and filtered, and the filtrate was concen-

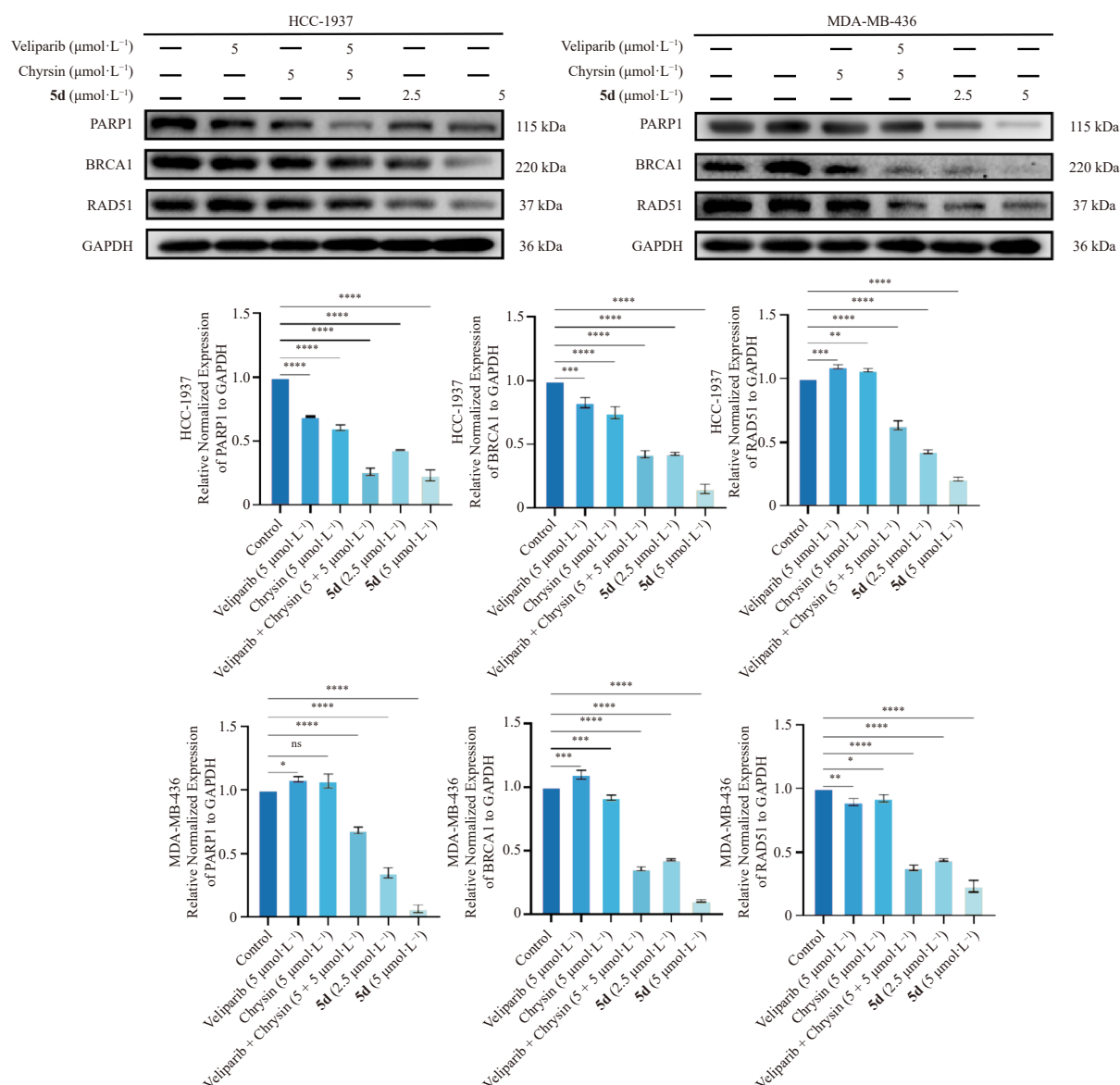


Fig. 5 Western blotting analysis of the expression of PARP1 and key enzymes in homologous recombination (HR) repair of DNA damage (BRCA1 and RAD51) levels in the cells treated with 5d. GAPDH was used as a loading control. The error bar indicated the SD, * $P < 0.05$, ** $P < 0.01$, *** $P < 0.001$, and **** $P < 0.0001$ vs the control groups.

trated. The residue was then purified by column chromatography on silica gel using a petroleum ether/ethyl acetate (10 : 1) mixture, yielding a yellow solid intermediate. This intermediate was dissolved in methanol (70 mL) and adjusted to pH 10.0. The mixture was stirred until TLC confirmed complete conversion. Subsequently, the pH was adjusted to 3.0 using dilute hydrochloric acid, followed by filtration. The residue was washed with dilute hydrochloric acid, saturated sodium chloride solution, and water, respectively. The product, a yellow residue (**3a**), was dried in a vacuum oven at 45 °C to obtain 1.79 g, representing an 86% yield.

In Step 2, compound **3a** (0.1 mmol) was mixed with HATU (0.1 mmol), 2,3-diaminobenzamide (0.11 mmol), and DIPEA (0.2 mmol) in DMF (10 mL). The mixture was stirred at room temperature for 20 h. After completion, it was poured

into ice-cold water (100 mL), and the solid product was filtered out. This product was dissolved in acetic acid (30 mL) and refluxed at 120 °C for 18 h. The reaction mixture was then cooled to 25 °C, poured into ice water, and extracted with ethyl acetate (3 × 20 mL). The combined organic layers were washed with saturated sodium salt water, dried with anhydrous MgSO₄, and concentrated under reduced pressure. The crude product was purified by silica gel chromatography (methylene chloride/methanol, 20 : 1) to yield a pale pink solid (**5a**, 0.24 g, 38% yield), with a melting point of 248.2–251.0 °C. The compound's structure was confirmed by ¹H NMR (400 MHz, DMSO-*d*₆) showing signals at δ 12.84 (s, 1H), 9.36 (s, 1H), 8.39–8.19 (m, 2H), 8.09 (s, 1H), 7.96–7.30 (m, 10H), 7.03 (s, 1H), 6.53 (s, 1H), 5.17 (s, 2H). ¹³C NMR (101 MHz, DMSO) with peaks at δ 182.53, 172.53,

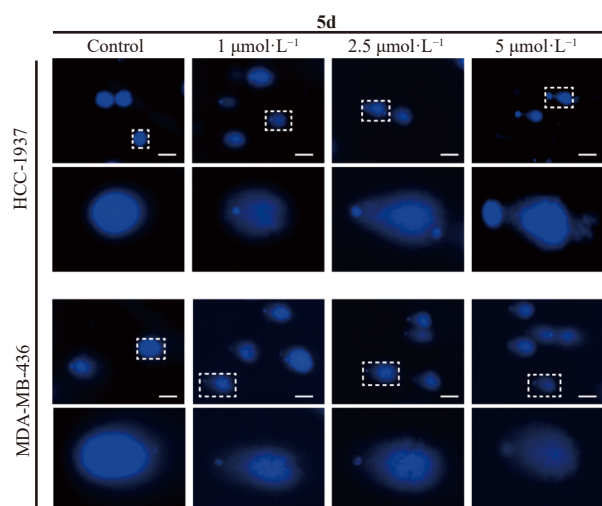


Fig. 6 Compound 5d-mediated defects in DNA repair. Investigation of DNA damage in the cells caused by 5d (1, 2.5, and 5 $\mu\text{mol}\cdot\text{L}^{-1}$). The alkaline comet assay was applied to detect the extent of DNA damage. Scale bar = 10 $\mu\text{mol}\cdot\text{L}^{-1}$.

and so on, down to 70.01. The compound's high-resolution mass spectrometry (HRMS) (ESI) data ($[M + H]^+$) showed a calculated (Calcd.) mass for $\text{C}_{30}\text{H}_{22}\text{N}_3\text{O}_5$ of 504.1554, with a found mass of 504.1560.

2-(3-((5-hydroxy-4-oxo-2-phenyl-4H-chromen-7-yl)oxy)propyl)-1H-benzo[d]imidazole-4-carboxamide (**5b**)

White solid (yield 39%); mp 224.0–226.1 °C. ^1H NMR (400 MHz, $\text{DMSO}-d_6$) δ 12.71 (s, 1H), 7.98–7.95 (m, 2H), 7.83 (dd, $J = 7.6, 1.1$ Hz, 1H), 7.68 (d, $J = 7.8$ Hz, 2H), 7.59–7.45 (m, 3H), 7.26 (t, $J = 7.8$ Hz, 1H), 6.88 (s, 1H), 6.61 (d, $J = 2.2$ Hz, 1H), 6.24 (d, $J = 2.2$ Hz, 1H), 4.15 (t, $J = 6.3$ Hz, 2H), 3.10 (t, $J = 7.5$ Hz, 2H), 2.29 (p, $J = 6.7$ Hz, 2H). ^{13}C NMR (101 MHz, DMSO) δ 182.32, 172.55, 167.23, 164.87, 163.72, 161.50, 157.62, 156.07, 132.43, 130.91, 129.46, 126.73, 122.48, 121.82, 121.44, 116.23, 105.59, 105.27, 98.86, 93.42, 68.15, 27.14, 25.29, 21.54. HRMS (ESI) (m/z): $[M + \text{Na}]^+$ Calcd. for $\text{C}_{26}\text{H}_{21}\text{N}_3\text{NaO}_5$ 478.1373, found 478.1380.

2-(4-((5-hydroxy-4-oxo-2-phenyl-4H-chromen-7-yl)oxy)butyl)-1H-benzo[d]imidazole-4-carboxamide (**5c**)

Yellow solid (yield 50%); mp 230.8–232.4 °C. ^1H NMR (400 MHz, $\text{DMSO}-d_6$) δ 12.77 (s, 1H), 9.38 (s, 1H), 8.04 (d, $J = 6.9$ Hz, 2H), 7.88–7.47 (m, 6H), 7.25 (t, $J = 7.7$ Hz, 1H), 6.96 (s, 1H), 6.70 (s, 1H), 6.33 (s, 1H), 4.11 (s, 2H), 2.99 (t, $J = 7.3$ Hz, 2H), 1.97 (s, 2H), 1.84 (s, 2H). ^{13}C NMR (101 MHz, DMSO) δ 182.42, 172.50, 166.83, 165.08, 163.78, 161.59, 157.72, 156.44, 141.55, 134.98, 132.50, 131.04, 129.52, 126.83, 122.53, 122.30, 121.75, 114.92, 105.72,

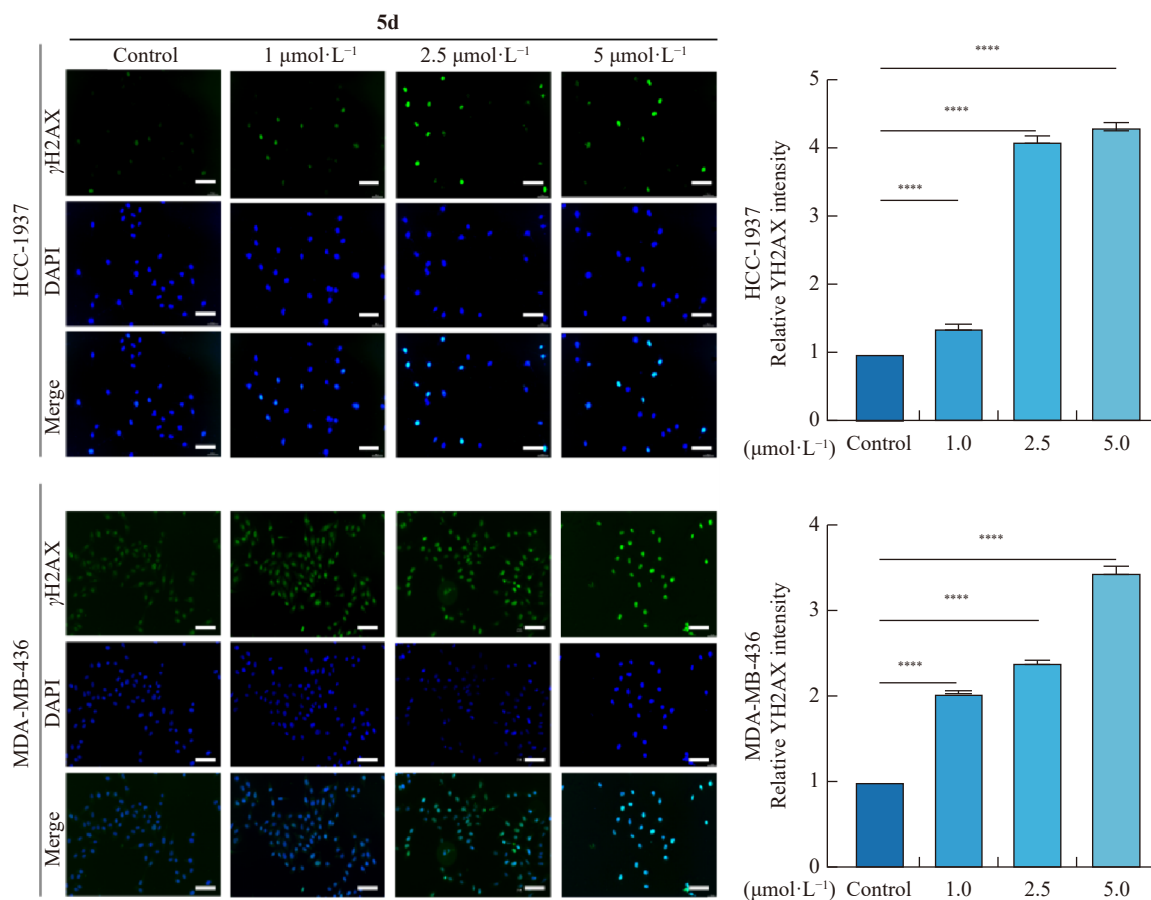


Fig. 7 Immunofluorescence analysis. The expression of the γH2AX in the cells treated with 5d for 48 h was determined. Scale bar = 20 $\mu\text{mol}\cdot\text{L}^{-1}$. The error bar indicated the SD; **** $P < 0.0001$ vs the control groups.

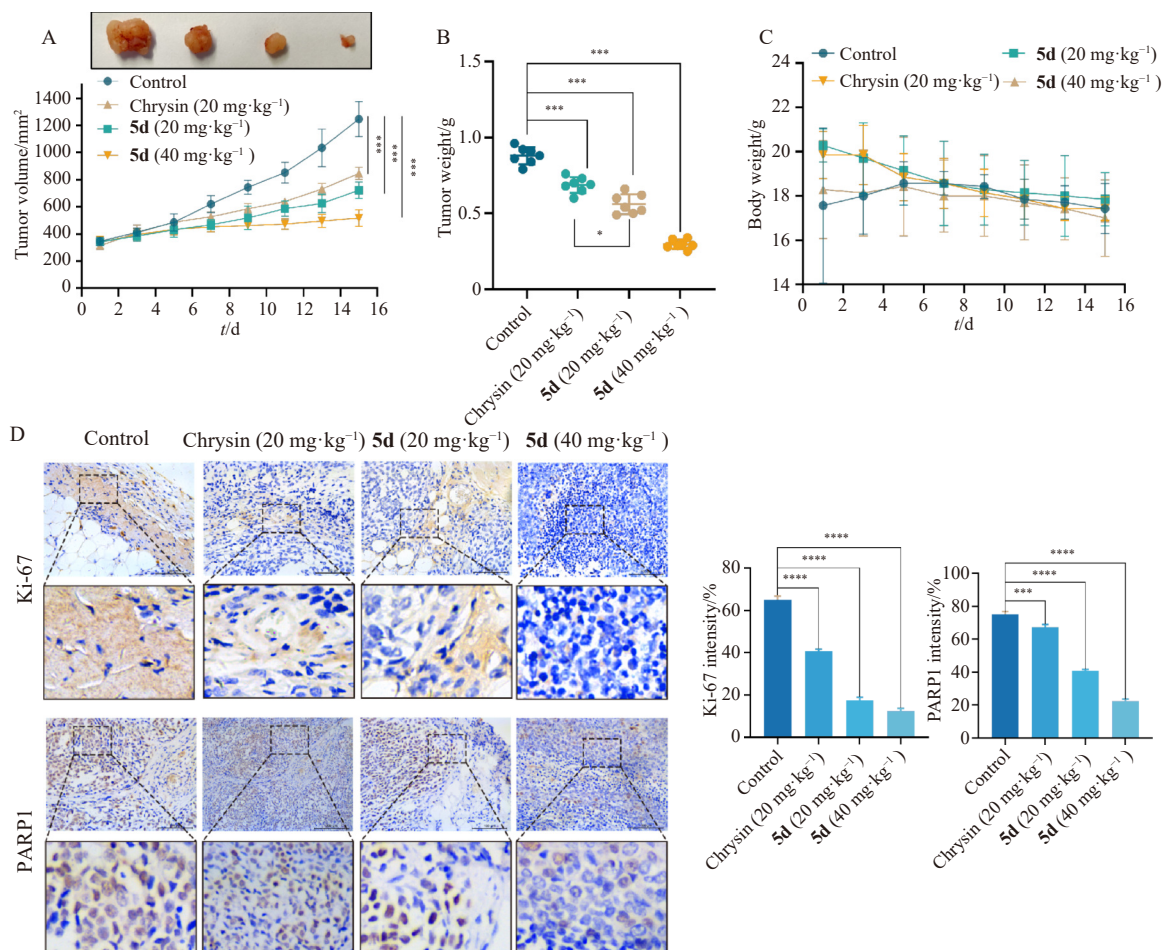


Fig. 8 Antitumor activities of **5d** on MDA-MB-436 xenograft models. (A) Tumor volume changes with oral administration of 20 or 40 mg·kg⁻¹ **5d** or 20 mg·kg⁻¹ chrysin; (B) Weight of tumor tissues at the end of therapy; (C) Changes of body weight in nude mice; (D) Representative images and quantitative analysis of IHC analysis of Ki-67 and PARP1 in different groups. Scale bar, 40 μmol·L⁻¹. The error bar showed the SD; **P* < 0.05, ****P* < 0.001, and *****P* < 0.0001 vs the control groups.

105.29, 98.89, 93.52, 68.57, 49.07, 28.46, 24.41, 21.51. HR-MS (ESI) (*m/z*): [M + Na]⁺ Calcd. for C₂₇H₂₃N₃NaO₅ 492.1530, found 492.1534.

2-(5-((5-hydroxy-4-oxo-2-phenyl-4H-chromen-7-yl)oxy)pentyl)-1H-benzo[d]imidazole-4-carboxamide (**5d**)

White solid (yield 44%); mp 243.7–245.9 °C. ¹H NMR (400 MHz, DMSO-*d*₆) δ 12.79 (s, 1H), 9.39 (s, 1H), 8.07 (d, *J* = 7.3 Hz, 2H), 7.92–7.47 (m, 6H), 7.26 (d, *J* = 7.9 Hz, 1H), 7.00 (s, 1H), 6.74 (s, 1H), 6.34 (d, *J* = 2.0 Hz, 1H), 4.09 (q, *J* = 11.1, 6.6 Hz, 2H), 2.95 (t, *J* = 7.5 Hz, 2H), 1.92–1.77 (m, 4H), 1.53 (q, *J* = 7.7 Hz, 2H). ¹³C NMR (101 MHz, DMSO) δ 182.45, 172.48, 166.83, 165.14, 163.80, 161.60, 157.75, 156.62, 141.58, 134.97, 132.52, 131.05, 129.54, 126.84, 122.49, 122.28, 121.71, 114.89, 105.73, 105.28, 98.87, 93.56, 68.79, 49.07, 28.82, 28.54, 27.63, 25.53, 21.51. HR-MS (ESI) (*m/z*): [M + Na]⁺ Calcd. for C₂₇H₂₃N₃NaO₅ 492.1530, found 492.1534.

2-(6-((5-hydroxy-4-oxo-2-phenyl-4H-chromen-7-yl)oxy)hexyl)-1H-benzo[d]imidazole-4-carboxamide (**5e**)

White solid (yield 40%); mp 267.0–268.2 °C. ¹H NMR (400 MHz, DMSO-*d*₆) δ 12.78 (s, 1H), 9.37 (s, 1H), 8.07 (d,

J = 7.2 Hz, 2H), 7.80 (d, *J* = 7.5 Hz, 1H), 7.73–7.48 (m, 5H), 7.25 (t, *J* = 7.7 Hz, 1H), 7.00 (s, 1H), 6.75 (s, 1H), 6.34 (s, 1H), 4.07 (d, *J* = 6.3 Hz, 2H), 2.91 (t, *J* = 7.5 Hz, 2H), 1.87–1.70 (m, 4H), 1.44 (q, *J* = 7.4, 6.4 Hz, 4H). ¹³C NMR (101 MHz, DMSO) δ 182.46, 172.48, 166.81, 165.19, 163.83, 161.60, 157.79, 156.70, 134.97, 132.54, 131.06, 129.56, 126.87, 122.47, 122.26, 121.69, 114.87, 105.75, 105.29, 98.90, 93.55, 68.90, 28.84, 28.79, 28.70, 27.81, 25.55, 21.52. HR-MS (ESI) (*m/z*): [M + Na]⁺ Calcd. for C₂₉H₂₇N₃NaO₅ 520.1843, found 520.1840.

Biology

Enzyme inhibitory activity assays

The inhibitory effects of the synthesized compounds on the PARP1 enzyme were evaluated by Shanghai ChemPartner Co., Ltd.

Cell culture and antibodies

Human breast cancer cell lines MDA-MB-231, MDA-MB-436, HCC-1937, and MCF-7 were acquired from the American Type Culture Collection (ATCC). These cells were maintained in Roswell Park Memorial Institute (RPMI) 1640 medium supplemented with 10% fetal bovine serum (FBS)

and 1% penicillin-streptomycin. Cultivation was performed at 37 °C in an atmosphere containing 5% CO₂. Antibodies used in the Western blotting assay included PARP1 (Abcam, No. ab191217), RAD51 (CST, No. 8875S), BRCA1 (CST, No. 9010), and GAPDH (CST, No. 5174), and Ki-67 (CST, No. 9027).

Cell viability assay

For the assessment of cell viability, human breast cancer cells were plated in 96-well plates at a density of 5 000 cells per well. Test compounds were prepared as 33.3 mmol·L⁻¹ stock solutions in DMSO. Following a 24-hour incubation at 37 °C, the cells were exposed to varying concentrations of the test compounds (ranging from 0 to 10 mmol·L⁻¹) for 48 h. The 3-(4,5-dimethylthiazol-2-yl)-2,5-diphenyltetrazolium bromide (MTT) assay was employed to determine the anti-proliferative effects of the synthesized molecules against cancer cells.

Colony formation assay

The colony formation assay was conducted to evaluate the proliferation potential of breast cancer cells upon treatment with the candidate molecule. Initially, 1 500 cells were seeded into each well of a six-well plate and incubated at 37 °C for 24 h. Subsequently, the cells were treated with the candidate molecule for ten days. Following treatment, the cells were fixed with 4% paraformaldehyde and stained with 0.5% crystal violet. Colony formation was quantified, with data represented as mean ± standard deviation (SD) from three independent experiments.

Wound healing assay

The wound healing assay was performed in accordance with previously described methods [22]. To evaluate cell migration, breast cancer cells were cultured to confluence in six-well plates and then mechanically wounded using sterilized pipettes. Cells were serum-starved before and after wounding to minimize proliferation effects. After a single wash with cold phosphate-buffered saline (PBS), the cells were treated with either the candidate molecule or normal medium. After 24 h of incubation at 37 °C, cell migration into the wounded area was documented using an inverted microscope.

Flow cytometry assay

According to the manufacture's instructions, the cell cycle process and the apoptotic ratio after candidate molecule treatment were evaluated using the cell cycle and apoptosis kit (Beyotime Biotechnology, Jiangsu, China) and Annexin-V-FLUOS staining kit (Roche, Germany), respectively. Next, a flow cytometer (BD FACS Calibur) was used to investigate cell cycle distribution and cell apoptosis. Data were processed using FlowJo software, and statistical analysis was conducted using GraphPad Prism 8.0 software.

Western blotting assay

Breast cancer cells were treated with various concentrations of the candidate molecule in six-well plates for two days. Following treatment, cells were washed twice with cold PBS and lysed. The lysates were centrifuged at 13 000 r·min⁻¹ at 4 °C for 20 min, and the protein concentrations

were determined using an enhanced bicinchoninic acid (BCA) protein assay kit (Beyotime Biotechnology, Jiangsu, China). Proteins were then separated by 15% sodium dodecyl sulfate-polyacrylamide gel electrophoresis (SDS-PAGE) and transferred onto nitrocellulose membranes. These membranes were blocked with 5% skim milk overnight and incubated with primary antibodies, followed by TBST washes and incubation with HRP-conjugated secondary antibodies. Protein bands were visualized using an ECL chemiluminescent HRP substrate.

Molecular docking

The Accelrys Discovery Studio (version 3.5; Accelrys, San Diego, CA, USA) software was employed for preparing the chemical molecule models. The candidate molecule's energy was minimized using a CHARMM force field before docking into the PARP1 active site (PDB code: 7KK6). Images of the docking positions were generated using PyMOL.

MDA-MB-436 xenograft tumor model

The animal experiments were carried out in strict accordance with the guidelines approved by the animal experimental research ethics committee of the University of South China. Forty female nude mice (BALB/c, aged 6–8 weeks, weighing 19–23 g) received subcutaneous injections of MDA-MB-436 cells (2.0 × 10⁶ cells per mouse). Once the tumors reached a volume of 100–200 mm³ (calculated as $V = L \times W^2/2$), the mice were randomly assigned to one of four groups: a vehicle control group, a chrysin-treated group (20 mg·kg⁻¹·day, dissolved in 5% V/V dimethyl sulfoxide, 35% W/V 2-hydroxypropyl-β-cyclodextrin, and 60% normal saline), and two **5d**-treated groups (receiving 20 or 40 mg·kg⁻¹·day, suspended in 5% V/V dimethyl sulfoxide, 20% W/V sulfobutylether-β-cyclodextrin, and 75% normal saline). The chrysin and **5d** treatments were administered orally once daily for 21 d. Throughout the experiment, the tumor sizes and body weights of the mice were monitored and recorded every three days. Following the final treatment, the mice were euthanized, and their tumor tissues were collected for subsequent analysis.

Immunohistochemistry (IHC) analysis

For antigen retrieval, tumor sections were immersed in EDTA antigen retrieval buffer (pH 8.0) or citrate buffer (pH 6.0) and heated in a microwave. Sections were then incubated with anti-Ki-67 (1 : 500) or anti-PARP1 (1 : 500) antibodies at 37 °C for 30 min. HRP-conjugated secondary antibodies were applied before counterstaining with Meyer's hematoxylin.

Immunofluorescence analysis

Cells were cultured on glass coverslips in 24-well plates and treated with **5d**. Following fixation with 4% paraformaldehyde and permeabilization with 1% Triton X-100, cells were washed and incubated with specific primary antibodies overnight at 4 °C. After a PBS wash, samples were treated with the appropriate secondary antibody at 25 °C for 60 min. Nuclei were stained with DAPI for 10 min, and images were captured using a Zeiss LSM880 confocal microscope.

Conclusion

Currently, natural products are invaluable resources for discovering novel lead molecules for cancer treatment. Although chrysin displays a broad spectrum of biological activities, it suffers from poor water solubility and low bioavailability. Consequently, structural modifications of chrysin present a promising approach to developing potential therapeutic agents. In this study, by incorporating the key pharmacophore of the PARP1 inhibitor veliparib, we have identified a new series of chrysin-based PARP inhibitors that show promising inhibitory effects on PARP1 and BRCA-deficient breast cancer cells. Among these derivatives, compound **5d** demonstrated the most potent inhibitory activities against PARP1 and MDA-MB-436 cells, with IC₅₀ values of 108 nmol·L⁻¹ and 4.5 μmol·L⁻¹, respectively. Further *in vitro* and *in vivo* studies confirmed that **5d** significantly inhibited the growth of BRCA-deficient breast cancer cells by suppressing PARP1 expression. Overall, this research offers a novel approach to the development of new chrysin-based bioactive compounds.

References

- [1] Atanasov AG, Zotchev SB, Dirsch VM, *et al.* Natural products in drug discovery: advances and opportunities [J]. *Nat Rev Drug Discov*, 2021, **20**(3): 200-216.
- [2] Thomford NE, Senthebane DA, Rowe A, *et al.* Natural products for drug discovery in the 21st century: innovations for novel drug discovery [J]. *Int J Mol Sci*, 2018, **19**(6): 1578.
- [3] Mani R, Natesan V. Chrysin: sources, beneficial pharmacological activities, and molecular mechanism of actions [J]. *Phytochemistry*, 2018, **145**: 187-196.
- [4] Stompór-Gorący M, Bajek-Bil A, Machaczka M. Chrysin: perspectives on contemporary status and future possibilities as pro-health agents [J]. *Nutrients*, 2021, **13**(6): 2038.
- [5] Li Y, Li Y, He J, *et al.* The relationship between pharmacological properties and structure-activity of chrysin derivatives [J]. *Mini-Rev Med Chem*, 2019, **19**(7): 555-568.
- [6] Dewi RM, Megawati M, Antika LD. Antidiabetic properties of dietary chrysin: a cellular mechanism review [J]. *Mini Rev Med Chem*, 2022, **22**(10): 1450-1457.
- [7] Chen J, Wang Y, Zhao D, *et al.* Chrysin serves as a novel inhibitor of DGKα/FAK interaction to suppress the malignancy of esophageal squamous cell carcinoma (ESCC) [J]. *Acta Pharm Sin B*, 2021, **11**(1): 143-155.
- [8] Zhong X, Liu D, Jiang Z, *et al.* Chrysin induced cell apoptosis and inhibited invasion through regulation of TET1 expression in gastric cancer cells [J]. *OncoTargets Ther*, 2020, **13**: 3277-3287.
- [9] Chen N, Wang R, Lu L J, *et al.* Synthesis of chrysin derivatives and screening of antitumor activity [J]. *J Asian Nat Prod Res*, 2019, **22**(5): 1-8.
- [10] Li Y, Zhang Q, He J, *et al.* Synthesis and biological evaluation of amino acid derivatives containing chrysin that induce apoptosis [J]. *Nat Prod Res*, 2021, **35**(4): 529-538.
- [11] Liu YM, Li Y, *et al.* Design, synthesis, and preliminary biological evaluation of chrysin amino acid derivatives that induce apoptosis and suppress cell migration [J]. *J Asian Nat Prod Res*, 2020, **22**(6): 547-561.
- [12] Ali AM, Tawfik SS, Mostafa AS, *et al.* Benzimidazole-based protein kinase inhibitors: current perspectives in targeted cancer therapy [J]. *Chem Biol Drug Des*, 2022, **100**(5): 656-673.
- [13] Alzhurani ZMM, Alam MM, Nazreen S. Recent advancements on benzimidazole: a versatile scaffold in medicinal chemistry [J]. *Mini Rev Med Chem*, 2022, **22**(2): 365-386.
- [14] Pietanza MC, Waqar SN, Krug LM, *et al.* Randomized, double-blind, phase II study of temozolomide in combination with either veliparib or placebo in patients with relapsed-sensitive or refractory small-cell lung cancer [J]. *J Clin Oncol*, 2018, **36**(23): 2386-2394.
- [15] Boussios S, Karihtala P, Moschetta M, *et al.* Veliparib in ovarian cancer: a new synthetically lethal therapeutic approach [J]. *Invest New Drugs*, 2020, **38**(1): 181-193.
- [16] George RR, Thomas R, Davice A, *et al.* Veliparib for the treatment of solid malignancies [J]. *J Oncol Pharm Pract*, 2022, **28**(4): 924-934.
- [17] Lord CJ, Ashworth A. PARP inhibitors: synthetic lethality in the clinic [J]. *Science*, 2017, **355**(6330): 1152-1158.
- [18] Yin L, Liu Y, Peng Y, *et al.* PARP inhibitor veliparib and HDAC inhibitor SAHA synergistically co-target the UHRF1/BRCA1 DNA damage repair complex in prostate cancer cells [J]. *J Exp Clin Cancer Res*, 2018, **37**(1): 153.
- [19] Zang J, Liang X, Huang Y, *et al.* Discovery of novel pazopanib-based HDAC and VEGFR dual inhibitors targeting cancer epigenetics and angiogenesis simultaneously [J]. *J Med Chem*, 2018, **61**(12): 5304-5322.
- [20] Collins AR. Measuring oxidative damage to DNA and its repair with the comet assays [J]. *Biochim Biophys Acta*, 2014, **1840**(2): 794-800.
- [21] Turcotte V, Fortin S, Vevey F, *et al.* Synthesis, biological evaluation, and structure-activity relationships of novel substituted N-phenyl ureidobenzenesulfonate derivatives blocking cell cycle progression in S-phase and inducing DNA double-strand breaks [J]. *J Med Chem*, 2012, **55**(13): 6194-6208.
- [22] Cheng C, Ji Z, Sheng Y, *et al.* Aphthous ulcer drug inhibits prostate tumor metastasis by targeting IKKε/TBK1/NF-κB signaling [J]. *Theranostics*, 2018, **8**(17): 4633-4648.

Cite this article as: YANG Yao, TONG Jing, XIE Xianshun, *et al.* Design, synthesis, and biological evaluation of novel chrysin derivatives as poly(ADP-ribose) polymerase 1 (PARP1) inhibitors for the treatment of breast cancer [J]. *Chin J Nat Med*, 2024, **22**(5): 455-465.